Article

XPS and NEXAFS Studies of Zn-Doped Bismuth Iron Tantalate Pyrochlore

Sergey V. Nekipelov [1,*], Victor N. Sivkov [1], Danil V. Sivkov [1], Alexey M. Lebedev [2], Ratibor G. Chumakov [2], Aleksandra V. Koroleva [3], Boris A. Makeev [4] and Nadezhda A. Zhuk [5]

[1] Institute of Physics and Mathematics, Komi Science Center UB RAS, Oplesnina St. 4, Syktyvkar 167982, Russia; sivkovvn@mail.ru (V.N.S.)

[2] National Research Center, Kurchatov Institute, 1 Akad. Kurchatova Sq., Moscow 123182, Russia; lebedev.alex.m@gmail.com (A.M.L.); ratibor.chumakov@gmail.com (R.G.C.)

[3] Faculty of Physics, Saint Petersburg State University, University Emb. 7/9, St. Petersburg 199034, Russia; koroleva.alexandra.22@gmail.com

[4] Institute of Geology, Komi Science Center UB RAS, Pervomaiskaya St. 48, Syktyvkar 167982, Russia; makboris@mail.ru

[5] Institute of Natural Sciences, Syktyvkar State University, Oktyabrsky Prospect, 55, Syktyvkar 167001, Russia; nzhuck@mail.ru

* Correspondence: nekipelovsv@mail.ru

Abstract: The effect of Zn-doping on the phase composition and optical properties of the $Bi_2Zn_xFe_{1-x}Ta_2O_{9.5-\Delta}$ (x = 0.3, 0.5, 0.7) was studied. XRD data showed that the samples crystallize in the structural type of pyrochlore (sp. gr.Fd-3m). For all the samples, an admixture of bismuth orthotantalate β-BiTaO$_4$ triclinic modification up to 22.5 wt.% is observed. The content of β-BiTaO$_4$ increases with zinc doping. The unit cell parameter of the pyrochlore phase rises from 10.4878 (x = 0.3) to 10.5154 Å (x = 0.7). The samples are characterized by a porous microstructure with indistinct grain boundaries. Zinc oxide has a sintering effect on ceramics. The charge state of the ions in $Bi_2Zn_xFe_{1-x}Ta_2O_{9.5-\Delta}$ was investigated by X-ray spectroscopy. NEXAFS and XPS data show that zinc doping does not change the oxidation degree of iron and bismuth ions in pyrochlore. The ions are in the charge states Bi(+3), Fe(+3), Zn(+2). In the Ta4fspectrum, an energy shift of the absorption band towards lower energies by ΔE = 0.5 eV is observed, which is typical for tantalum ions with an effective charge of (+5-δ). With the increase of x(Zn), the Bi $4f_{7/2}$ and Bi $4f_{5/2}$ bands are observed to shift to lower energies due to the distribution of some Zn(II) ions in the bismuth position.

Keywords: pyrochlore; Zn-doping; BiTaO$_4$; XPS and NEXAFS spectroscopy

1. Introduction

Oxide compounds with pyrochlore structure attract close attention of scientists due to their wide range of practically useful properties, such as photocatalytic, dielectric, and semiconducting ones [1–3]. They exhibit ferro- and ferrimagnetism, superconductivity, and the spin glass state [4–6]. Traditionally, binary oxide pyrochlores are described by the general formula $A_2B_2O_7$ with a combination of three- and four- $(A^{3+}_2B^{+4}_2O_7)$ or two- and five-valent elements $(A^{2+}_2B^{+5}_2O_7)$ in the cationic sublattices A and B [7]. The cubic structure of pyrochlores is formed by two interpenetrating octahedral, framework B_2O_6 and tetrahedral A_2O' sublattices. Relatively small cations (Ti^{4+}, Ta^{5+}) occupy cation positions B. The large ions A (Ca^{2+}, Bi^{3+}) are arranged in the octagonal polyhedron formed by the oxygen atoms of the $A_2O'$and B_2O_6 sublattices [8–11]. The flexibility of the crystal structure to substitutions of cations in both sublattices and vacancies in the anion sublattice allows the chemical composition of pyrochlores to vary considerably in order to obtain compounds with different physicochemical properties. Mixed pyrochlores doped with transition element ions are being actively studied [12–23]. A distinctive feature of such pyrochlores is

the placement of some transition metal cations (B'–Zn, Cu, Co, Mn) on two non-equivalent cationic sublattices A and, to a greater extent, in the position B. This leads to the formation of a bismuth-defective pyrochlore structure. The chemical formula for the three-element pyrochlores can be represented as $(AB')_2(B'B)_2O_{7-\delta}$. The reason for the placement of B' ions in the A ion sublattice is associated with the stress of octahedral framework $(BB')_2O_6$ caused by oxygen vacancies due to the placement of heterovalent and dopant ions disproportionate to the B sublattice ions [24]. In the present work, we investigate, for the first time, bismuth-containing pyrochlores of a more complex composition containing two types of 3Delements, iron and zinc. The active interest of scientists in iron-containing pyrochlores is due to the discovery of their photocatalytic activity depending on the concentration of iron(III) ions, effect of the spin glass state, and excellent dielectric properties [15,19–21,25–31]. It was shown that pyrochlores in the Bi_2O_3-Fe_2O_3-Nb_2O_5 system exhibit dielectric permittivity of 141–151 and dielectric losses are close to the value of 0.2 at 30 °C and 1 MHz [30]. For $Bi_{1.657}Fe_{1.092}Nb_{1.150}O_7$ pyrochlore, the dielectric constant remains high ~120 at 300 K and 1 MHz [21]. The iron-containing pyrochlores $Bi_{3.36}Fe_{2.08+x}Ta_{2.56-x}O_{14.56-x}$ ($-0.32 \leq x \leq 0.48$) are characterized by lower values of dielectric permittivity ~78–92 and dielectric loss tangent ~10-1 (MHz, ~30 °C) [25]. Meanwhile, $Bi_{3.36}Fe_{2.08+x}Sb_{2.56-x}O_{14.56-x}$ ($0 \leq x \leq 0.64$) samples have more underestimated dielectric permittivity values in the range of 24–35 and dielectric losses of order 10-1 at room temperature (RT) and 1 MHz [31]. The dielectric permittivity of $Bi_2Mg_xFe_{1-x}Ta_2O_{9.5\pm\Delta}$ solid solutions increases with increasing iron content from 28.5 to 30.5, and the dielectric loss tangent does not exceed 0.001 (at 20 °C, 1 MHz) [32]. Based on magnetic susceptibility data, Mössbauer spectroscopy, and EELS analysis of iron-containing pyrochlores, it was found that iron ions are in the high-spin state of Fe(III), occupying predominantly octahedral Nb/Ta/Sb positions [15,19–21,25–31]. It was shown that the fraction of iron(III) cations in the A positions can vary from 4% to 25% [19,21,29]. For example, in the Bi_2O_3-Fe_2O_3-Nb_2O_5 pyrochlores only 4–15% of the A positions are occupied by Fe^{3+} ions [21]. In our work, we demonstrated the possibility of formation of Zn, Fe codoped bismuth tantalate pyrochlores and investigated the influence of zinc ions on the structure and charge state of the ions in the pyrochlore.

2. Experimental

The samples $Bi_2Zn_xFe_{1-x}Ta_2O_{9.5-\Delta}$ (x = 0.3, 0.5, 0.7) were synthesized by solid-phase reaction [32] from ZnO, Bi_2O_3, Fe_2O_3, and Ta_2O_5 oxides. The synthesis was carried out in stages at 650, 850, 950, and 1050 °C for 10 h at each calcination stage. Methods of scanning electron microscopy and energy dispersive X-ray spectroscopy (electron scanning microscope Tescan VEGA 3LMN, energy dispersion spectrometer INCA Energy 450 (Tescan, Czech)) were used to investigate the microstructure and the local elemental composition of samples. X-ray photoelectron spectroscopy (XPS) studies were carried out using the equipment of the resource center of the Scientific Park of St. Petersburg State University "Physical methods of surface research" (St. Petersburg, Russia). XPS analysis was performed on a Thermo Scientific ESCALAB 250Xi X-ray spectrometer (Escalab 250Xi, Thermo Fisher Scientific, United Kingdom, Avantage v5.9925)). An AlKα X-ray tube (1486.6 eV) was used as an ionizing radiation source. To neutralize the sample charge, an ion-electron charge compensation system was used. All peaks were energy calibrated by the C 1s peak at 284.6 eV. The experimental data were processed using the ESCALAB 250Xi spectrometer software. The samples were also investigated by near edge X-ray absorption fine structure (NEXAFS) spectroscopy at the NanoPES station of the KISI synchrotron radiation source at the Kurchatov Institute (Moscow, Russia) [33]. NEXAFS spectra were measured in the total electron yield (TEY) mode with an energy resolution of 0.6 eV.

3. Results and Discussion

Based on the X-ray phase analysis, it was found that the samples of $Bi_2Zn_xFe_{1-x}Ta_2O_{9.5-\Delta}$ (x = 0.3, 0.5, 0.7), in contrast to similar magnesium compositions, are two-phase [32]. In addition to the main cubic phase, they contain bismuth orthotantalate of triclinic modification

as an impurity [34]. Analysis of the extinguishing reflections of the cubic phase confirmed that the symmetry of the crystal structure is cubic with the spatial group Fd-3 m [7]. The quantitative estimation of the bismuth orthotantalate content showed that the impurity content varies from 15.9 (x = 0.3) to 22.5 wt.% (x = 0.7) and increases with increasing zinc content in the samples. Apparently, the appearance of the impurity in the samples is associated with the placement of Zn(II) ions rather than iron(III) ions at the two cationic positions of bismuth(III) and tantalum(V), which is caused by their larger size and preference of zinc(II) ions for tetrahedral coordination. The closeness of the polarization properties and ionic radii of Fe(III) and Ta(V) (R(Fe(III))c.n-6 = 0.645 Å, R(Ta(V))c.n-6 = 0.64 Å) [35] explains the preference of Fe(III) ions for octahedral positions, repeatedly proven by physical and chemical analysis methods [26,36,37]. The large radius of zinc cations causes distortion of the octahedral framework and transfer of some of the zinc ions to the bismuth positions. Bismuth, in order to provide the vacancies of the sublattice, is isolated as an impurity of bismuth orthotantalate. A similar mechanism of pyrochlore structure interaction with dopant ions was first discovered and described in [24]. The differences from the magnesium compositions are due to the greater radius of zinc ions as compared to magnesium ions (R(Mg(II))c.n-6 = 0.72 Å, R(Zn(II))c.n-6 = 0.74 Å). Because of this, magnesium ions in $Bi_2Mg_xFe_{1-x}Ta_2O_{9.5-\Delta}$ solid solutions predominantly remain in octahedral positions. It is interesting to note that while the magnesium and zinc have the same charge and close ionic radius in the six- and eight-coordinated positions (R(Bi(III))c.n-8 = 1.17 Å, R(Mg(II))c.n-8 = 0.89 Å, R(Zn(II))c.n-8 = 0.90 Å), their distribution in the bismuth position is different. Apparently, the polarization properties of the ions have amain influence on it. In particular, the Allred–Rochov electronegativity of bismuth and zinc atoms coincide and are equal to 1.67, while the electronegativity of magnesium is substantially less, equal to 1.23, and closer to that of tantalum [38]. Calculation of the pyrochlore phase unit cell parameters has shown that with the zinc concentration growth the unit cell parameter linearly increases from 10.4878 (x = 0.3) to 10.5154 Å (x = 0.5), obeying the Vegard's rule (Figure 1). This fact indicates the uniform filling of the cationic sublattices with zinc and iron ions in the samples.
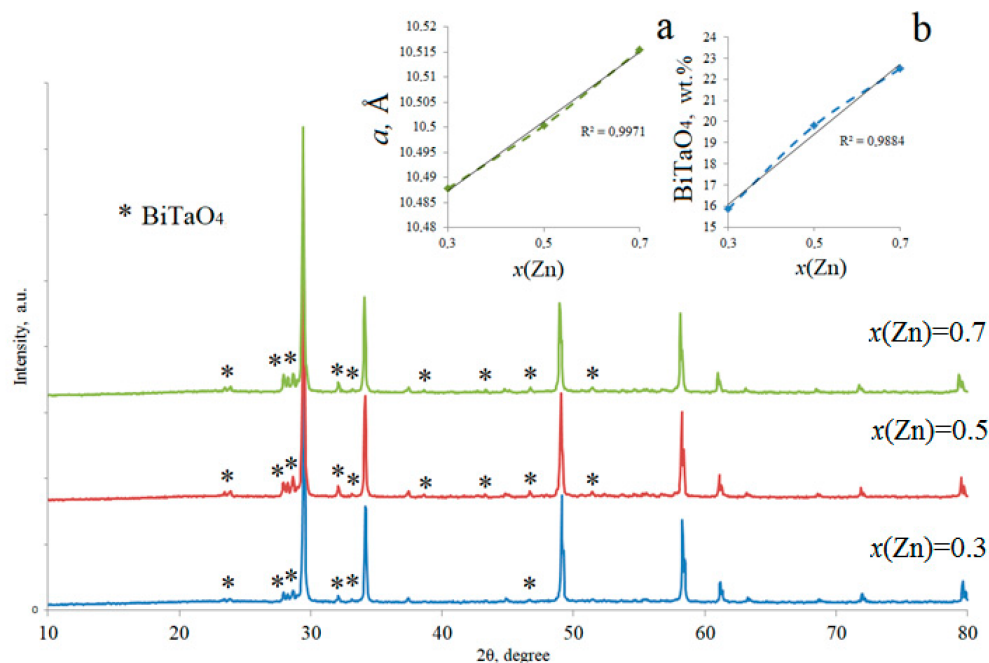
Figure 1. XRD patterns of the $Bi_2Zn_xFe_{1-x}Ta_2O_{9.5-\Delta}$ samples at different values of the x(Zn) index. Insets show the dependence of the unit cell parameter of pyrochlore (**a**) and the amount of BiTaO4 impurity (**b**) on the x(Zn) index.

It should be noted that the unit cell parameters of pyrochlore phase in $Bi_2Zn_xFe_{1-x}Ta_2O_{9.5-\Delta}$ agree with the unit cell parameter for $Bi_2FeTa_2O_{9.5}$, $a = 10.4871(2)$ Å [32], and are also close to the values for iron-containing pyrochlores based on tantalate $Bi_{3.36}Fe_{2.08+x}Ta_{2.56-x}O_{14.56-x}$ ($-0.32 \leq x \leq 0.48$) (10.4979–10.5033 Å) [25] and bismuth niobate ($Bi_{1.721}Fe_{0.190}(Fe_{0.866}Nb_{1.134})O_7$), $a = 10.508$ Å, and $Bi_{3.36}Fe_{2.08+x}Nb_{2.56-x}O_{14.56-x}$ ($-0.24 \leq x \leq 0.48$), for which the parameter varies from 10.5071(4) to 10.5107(7) Å [21,30].

According to scanning electron microscopy (SEM) data, $Bi_2Zn_xFe_{1-x}Ta_2O_{9.5-\Delta}$ samples are characterized by a porous microstructure, which consists of rounded partially fused grains with longitudinal size of 0.5–4 µm (Figures 2 and 3). Compared to Mg, Fe pyrochlores of similar composition, the samples are less porous and their grain size is 2–3 times larger. The influence of zinc on the ceramic density can also be traced by comparing the microstructure of ceramics without zinc using $Bi_2FeTa_2O_{9.5}$ and $Bi_2Fe_{0.3}Zn_{0.7}Ta_2O_9$ as examples. The photographs of the surface of $Bi_2FeTa_2O_{9.5}$ and $Bi_2Zn_{0.7}Fe_{0.3}ZnO_{9+y}$ samples are presented below. As can be seen from the microphotographs (Figure 2), the ceramics with zinc is characterized by a denser microstructure, has fewer pores, and is formed by melted ceramic grains of a large size.
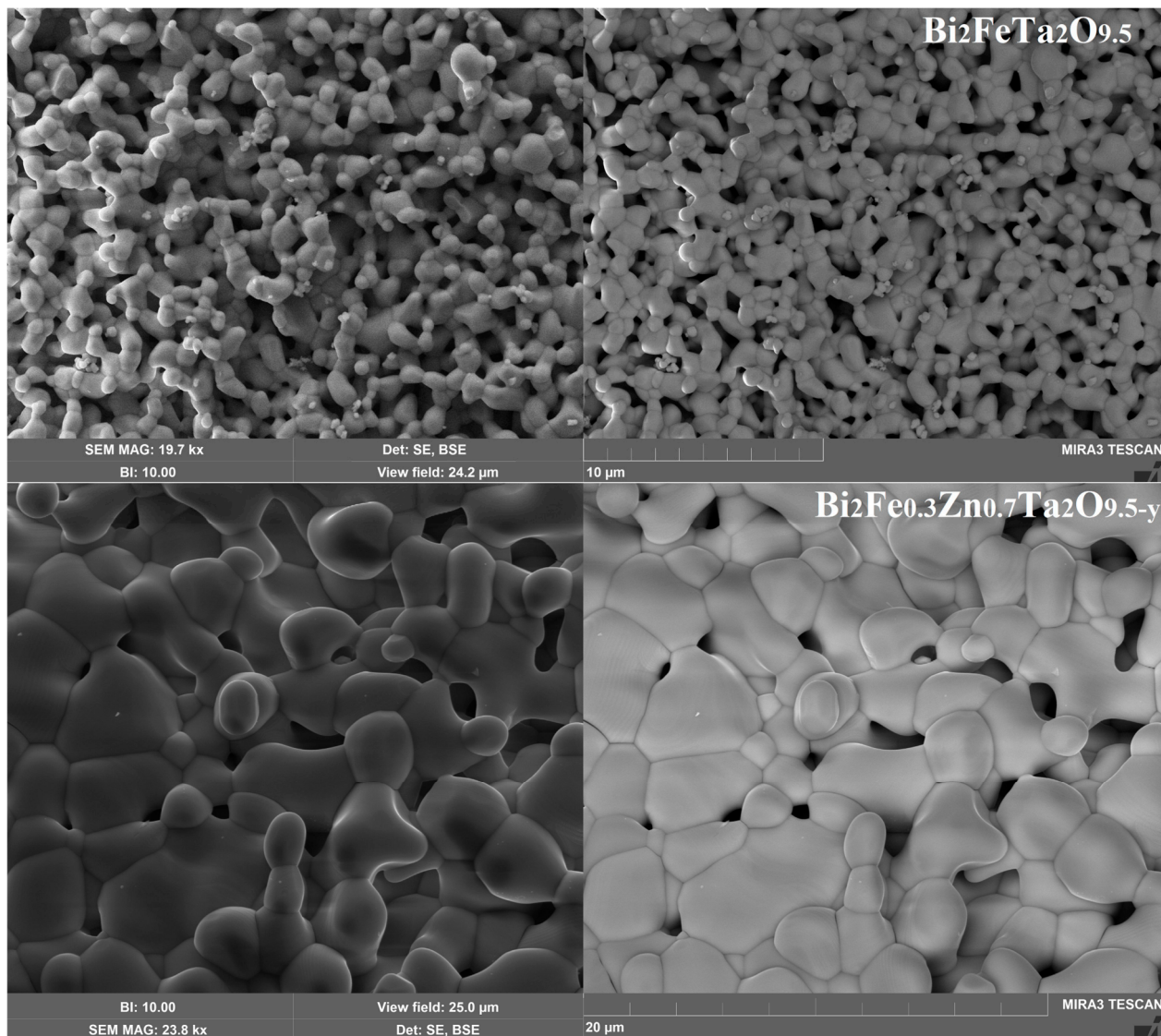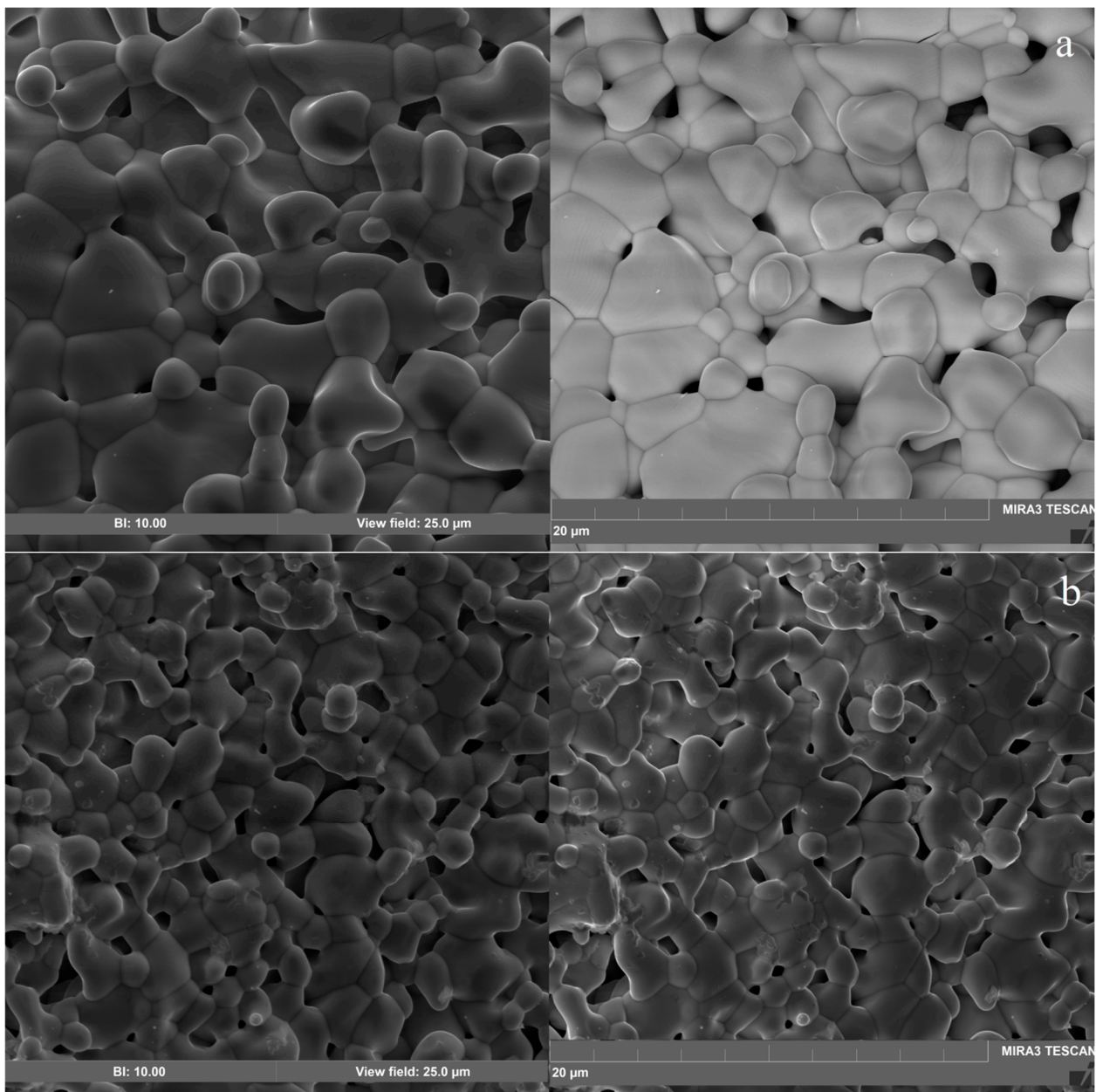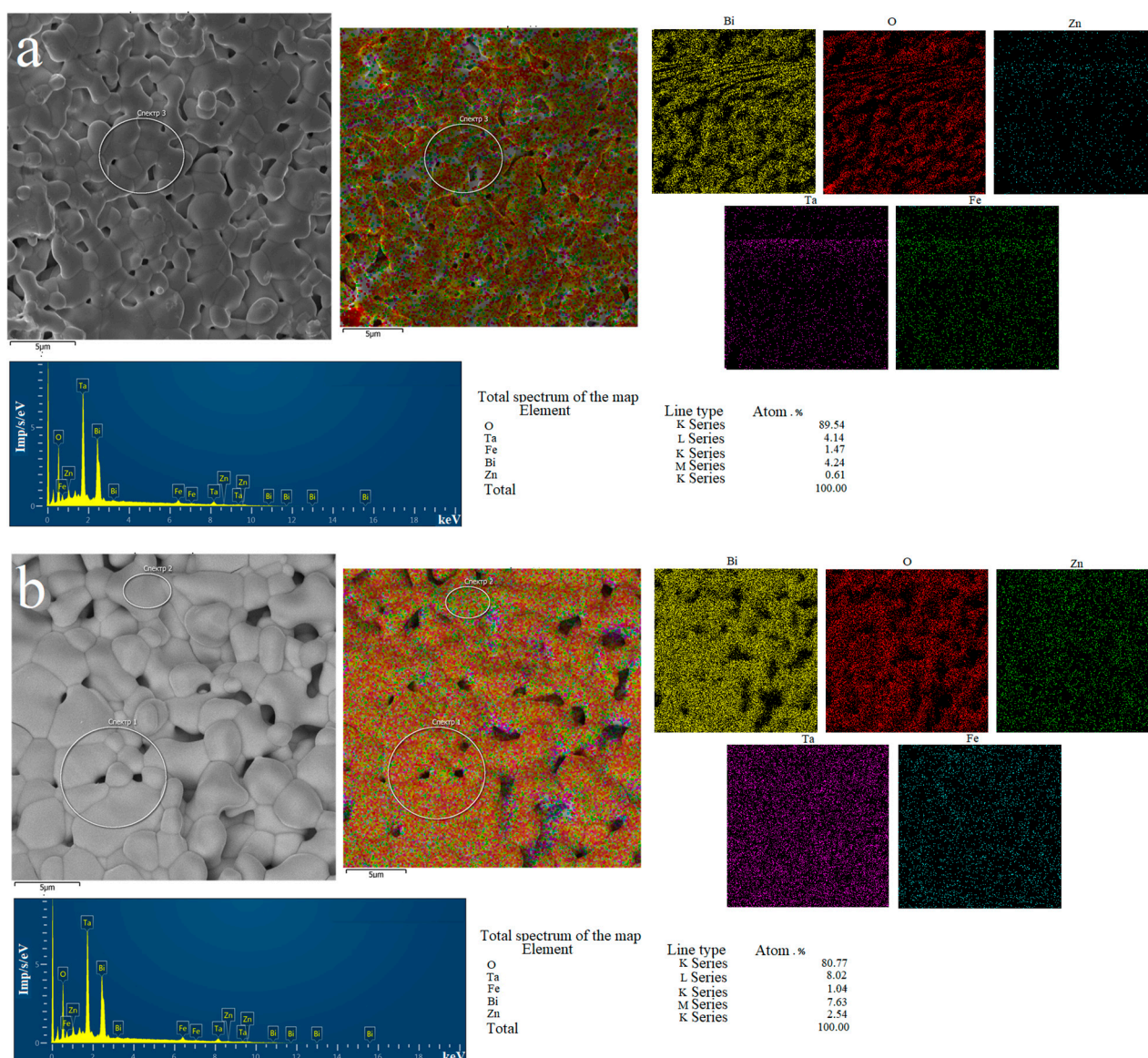

Figure 2. Microphotographs of $Bi_2FeTa_2O_{9.5}$ and $Bi_2Fe_{0.3}Zn_{0.7}Ta_2O_{9.5-y}$.

Figure 3. SEM microphotographs of the $Bi_2Zn_xFe_{1-x}Ta_2O_{9.5-\Delta}$ ceramic at x = 0.7 (**a**) and 0.3 (**b**) in the mode of secondary and elastically reflected electrons.

Local quantitative analysis by energy dispersive X-ray spectroscopy (EDS) showed that the experimental composition of the samples corresponded to the given. Elemental mapping of the samples showed a uniform distribution of zinc and iron atoms on the surface of the samples (Figures 3 and 4).

Figure 4. Microphotographs, EDS spectrum, and elemental mapping results of $Bi_2Fe_{0.7}Zn_{0.3}Ta_2O_9$ (**a**) and $Bi_2Fe_{0.3}Zn_{0.7}Ta_2O_9$ (**b**).

The electronic state of atoms in Zn, Fe-codoped bismuth tantalate pyrochlore was studied by NEXAFS and XPS spectroscopy (Figure 5). XPS was used to study the chemical state of the surface of the studied samples. XPS spectra of Fe, Zncodoped bismuth tantalate with varying molar ratio of Zn/Fe and corresponding oxides are shown in Figure 5a–e: XPS spectra in the wide energy range of binding energies (20–1400 eV) and spectral dependences around Bi 4f, Bi 5d, Ta 4f, Zn 2p, and Fe 2p thresholds of ionization. The plots show the results of decomposition of the spectral dependences into separate peaks modeled by Gauss–Lorentz curves and the background lines modeled by Shirley approximation. Only the spectra of metals were analyzed. This is because the Survey XPS spectrum captures the C 1s peak due to sample surface contamination, which can give an uncertain contribution to the O 1s peak intensity.
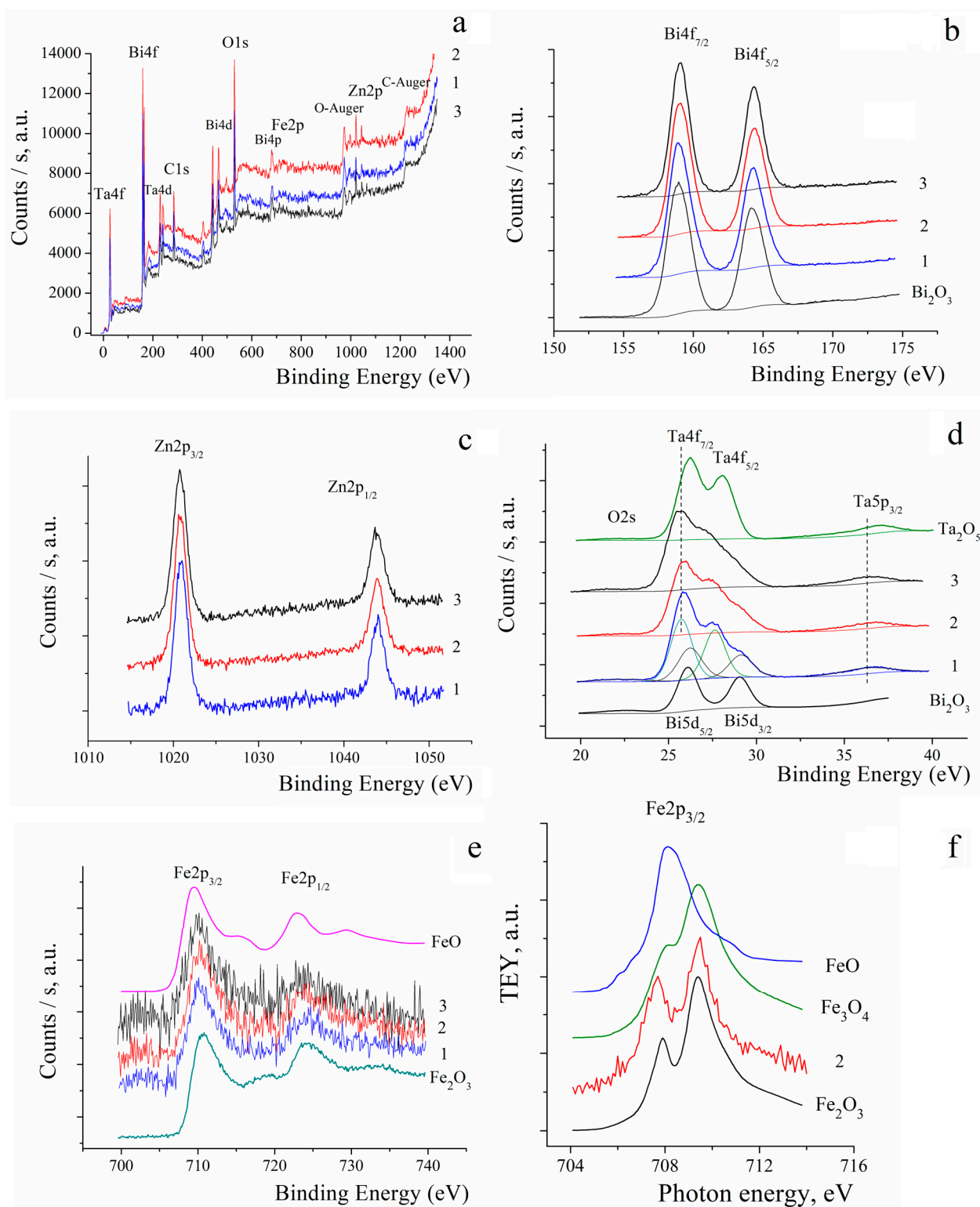
Figure 5. XPS spectra of $Bi_2Zn_xFe_{1-x}Ta_2O_{9.5-\Delta}$ at x = 0.7 (1), 0.5 (2), 0.3 (3): Survey (**a**), Bi4f– (**b**), Zn2p– (**c**), Ta4f– and Bi5d– (**d**), Fe2p– spectra (**e**); NEXAFS spectra of $Bi_2Zn_{0.5}Fe_{0.5}Ta_2O_{9.5-\Delta}$ and FeO [39], Fe_3O_4, Fe_2O_3 oxides (**f**).

First of all, it should be noted that the analyzed spectra are similar to the previously obtained spectra for pyrochlores of composition $Bi_2MTa_2O_9$ (M-Co, Ni, Fe), $Bi_2Mg_{1-x}Fe_xTa_2O_{9+\Delta}$ [23,24,26,32] in basic details and energy position. The energy positions of the components of the XPS spectra of $Bi_2Zn_xFe_{1-x}Ta_2O_{9.5-\Delta}$ are given in Table 1.

Table 1. Energy positions of the components of the XPS spectra of $Bi_2Zn_xFe_{1-x}Ta_2O_{9.5-\Delta}$: x = 0.7 (1), 0.5 (2), 0.3 (3).

Peak	Energy (eV)		
	1	2	3
$Bi4f_{7/2}$	159.03	159.08	159.09
$Bi4f_{5/2}$	164.34	164.4	164.42
$Bi5d_{5/2}$	26.35	26.29	26.3
$Bi5d_{3/2}$	29.25	29.19	29.2
$Ta4f_{7/2}$	25.87	25.81	25.81
$Ta4f_{5/2}$	27.77	27.71	27.71
$Zn2p_{3/2}$	1020.74	1020.8	1021.07
$Zn2p_{1/2}$	1043.75	1043.85	1044.12
$Fe2p_{3/2}$	709.99	710.15	710.19
$Fe2p_{1/2}$	723.35	723.45	723.83
Fe2p sat	718.05	718.44	718.79
Fe2p sat	731.55	731.65	731.74

The assignment of the observed spectrum components to chemical states was performed on the basis of literature data [39–44]. Some peculiarities of the new spectra should be noted. Doping with zinc atoms does not significantly change the spectral characteristics of bismuth, tantalum, and iron ions in pyrochlore as a whole (Figure 5).

This suggests that the degree of oxidation of the ions in the presented compounds remains unchanged. The energy position of the peaks in the XPS Bi 4f, Bi 5d, and Zn 2p spectra shown in Figure 5b,c are characteristic of the trivalent bismuth atom [40] and divalent zinc atom [41], which suggests that the charge states of these ions in the considered bismuth compounds are Bi3+ and Zn^{2+}, respectively. It is interesting to note that for a number of $Bi_2Zn_xFe_{1-x}Ta_2O_{9.5-\Delta}$, the Bi $4f_{7/2}$ and Bi $4f_{5/2}$ absorption bands are observed to shift with increasing x(Zn) to a lower energy region, which means that the total effective charge of bismuth ions decreases due to the placement of a significant proportion of zinc(II) ions in the bismuth position.

When considering the spectra of the tantalum atom (Figure 5d), one can note that in both the 4f and 5p spectra, the shape of the peaks clearly indicates that all the tantalum atoms are in the same charge state (no splitting and distortion of the peaks). The energy position of the peaks has a characteristic shift toward lower energies as compared with the binding energies for these levels in the pentavalent tantalum oxide Ta_2O_5 taken from literature data [42,43]. It is known that the shift towards lower energies is characteristic in the case of a decrease in the effective positive charge. In particular, for the presented Ta 4f spectra, the energy shift $\Delta E = 0.5$ eV. This suggests that the tantalum ions have the same effective charge +(5-δ). Since any change in the chemical environment of the element affects the spatial redistribution of the charge of its valence electrons and, as a consequence, the binding energy of the electrons. Apparently, the observed shift is due to the replacement of tantalum positions by zinc(II), iron(III) ions with a smaller effective charge.

Let us consider the XPS Fe 2p spectra shown in Figure 5e. The Fe 2p spectra in the samples show two broad bands of Fe $2p_{1/2}$ and Fe $2p_{3/2}$ levels with characteristic binding energies of ~710 eV (Fe $2p_{3/2}$), ~724 eV (Fe $2p_{1/2}$) (Table 1). A comparison of the noisy spectra of the composite with the spectra of FeO [44] and Fe_2O_3 oxides does not allow unambiguous comparison of the energy position of the peaks and the general appearance of the spectra with the spectra of oxides and, accordingly, unambiguous determination of the charge state of iron ions in composites. NEXAFS spectra of ions are more informative in this case. In the NEXAFS Fe $2p_{3/2}$ spectrum of $Bi_2Fe_{0.5}Zn_{0.5}Ta_2O_{9.5-\Delta}$ two broad lines, ~708 and 709 eV, appear. Both lines are correlating well with the spectrum of six-coordinated iron in iron(III) oxide by energy position and line shape. The previously studied iron pyrochlores with a $Bi_2FeTa_2O_{9.5}$ composition have a similar spectrum [29]. Thus, doping with doubly charged zinc ions does not cause a change in the degree of oxidation of iron(III) ions in bismuth tantalate-based pyrochlores.

4. Conclusions

According to X-ray phase analysis the samples of $Bi_2Zn_xFe_{1-x}Ta_2O_{9.5-\Delta}$ (x = 0.3, 0.5, 0.7) include not only the main pyrochlore phase, but also an admixture of bismuth orthotantalate of triclinic modification, the content of which in the samples increases with index x. Presumably, it is connected with the distribution of zinc ions in the cationic bismuth sublattice. This assumption is confirmed by the energy shift to the region of lower energies of bismuth absorption bands (Bi $4f_{7/2}$ and Bi $4f_{5/2}$). The microstructure of the sample is porous and formed by partially fused grains of 0.2–4 μm in size. Apparently, zinc ions have a sintering effect on the ceramics. NEXAFS and XPS data show that bismuth, iron, and zinc ions are in charge states Bi(+3), Fe(+3), Zn(+2), and zinc doping does not change the oxidation degree of iron(III) ions in pyrochlore. The characteristic shift of the absorption band in the Ta 4f spectrum to the region of lower energies is $\Delta E = 0.5$ eV. It was found that the tantalum ions have an effective charge Ta(+5-δ). Synthesized samples with high iron content have potential use for photocatalysis and are suitable as high-frequency dielectrics.

Author Contributions: Conceptualization, N.A.Z.; methodology, N.A.Z., S.V.N. and V.N.S.; formal analysis, D.V.S.; investigation, N.A.Z., S.V.N., A.V.K., A.M.L., R.G.C. and B.A.M.; resources, A.V.K., A.M.L., R.G.C. and B.A.M.; data curation, N.A.Z. and S.V.N.; writing—original draft preparation, N.A.Z. and S.V.N.; writing—review and editing, N.A.Z. and S.V.N.; visualization, N.A.Z. and S.V.N.; funding acquisition, S.V.N. and V.N.S. All authors have read and agreed to the published version of the manuscript.

References

1. Du, H.; Yao, X. Structural trends and dielectric properties of Bi-based pyrochlores. *J. Mater. Sci. Mater. Electron.* **2004**, *15*, 613–616. [CrossRef]
2. Murugesan, S.; Huda, M.N.; Yan, Y.; Al-Jassim, M.M.; Subramanian, V. Band-Engineered Bismuth Titanate Pyrochlores for Visible Light Photocatalysis. *J. Phys. Chem. C* **2010**, *114*, 10598–10605. [CrossRef]
3. Khaw, C.C.; Tan, K.B.; Lee, C.K. High temperature dielectric properties of cubic bismuth zinc tantalate. *Ceram. Intern.* **2009**, *35*, 1473–1480. [CrossRef]
4. Hiroi, Z.; Yamaura, J.-I.; Yonezawa, S.; Harima, H. Chemical trends of superconducting properties in pyrochlore oxides. *Phys. C Supercond. Appl.* **2007**, *460–462*, 20–27. [CrossRef]
5. Bongers, P.F.; van Meurs, E.R. Ferromagnetism in Compounds with Pyrochlore Structure. *J. Appl. Phys.* **1967**, *38*, 944–945. [CrossRef]
6. Greedan, J.E. Frustrated rare earth magnetism: Spin glasses, spin liquids and spin ices in pyrochlore oxides. *J. Alloys Compd.* **2006**, *408–412*, 444–455. [CrossRef]
7. Subramanian, M.A.; Aravamudan, G.; Rao, G.V.S. Oxide pyrochlores—A review. *Prog. Solid State Chem.* **1983**, *15*, 55–143. [CrossRef]
8. Pandey, J.; Shrivastava, V.; Nagarajan, R. Metastable $Bi_2Zr_2O_7$ with Pyrochlore-like Structure: Stabilization, Oxygen Ion Conductivity, and Catalytic Properties. *Inorg. Chem.* **2018**, *57*, 13667–13678. [CrossRef]
9. Miles, G.C.; West, A.R. Pyrochlore Phases in the System $ZnO-Bi_2O_3-Sb_2O_5$: I. Stoichiometries and Phase Equilibria. *J. Am. Ceram. Soc.* **2006**, *89*, 1042–1046. [CrossRef]
10. Matteucci, F.; Cruciani, G.; Dondi, M.; Baldi, G.; Barzanti, A. Crystal structural and optical properties of Cr-doped $Y_2Ti_2O_7$ and $Y_2Sn_2O_7$ pyrochlores. *Acta Mater.* **2007**, *55*, 2229–2238. [CrossRef]

11. Hector, A.L.; Wiggin, S.B. Synthesis and structural study of stoichiometric Bi2Ti2O7 pyrochlore. *J. Solid State Chem.* **2004**, *177*, 139–145. [CrossRef]

12. Tan, K.B.; Lee, C.K.; Zainal, Z.; Khaw, C.C.; Tan, Y.P.; Shaari, H. Reaction study and phase formation in Bi_2O_3-ZnO-Nb_2O_5 ternary system. *Pac. J. Sci. Technol.* **2008**, *9*, 468–479.

13. Vanderah, T.A.; Lufaso, M.W.; Adler, A.U.; Levin, I.; Nino, J.C.; Provenzano, V.; Schenck, P.K. Subsolidus phase equilibria and properties in the system Bi_2O_3:$Mn_2O_{3\pm x}$:Nb_2O_5. *J. Solid State Chem.* **2006**, *179*, 3467–3477. [CrossRef]

14. Vanderah, T.A.; Siegrist, T.; Lufaso, M.W.; Yeager, M.C.; Roth, R.S.; Nino, J.C.; Yates, S. Phase Formation and Properties in the System Bi_2O_3:$2CoO_{1+x}$:Nb_2O_5. *Eur. J. Inorg. Chem.* **2006**, *2006*, 4908–4914. [CrossRef]

15. Valant, M.; Babu, G.S.; Vrcon, M.; Kolodiazhnyi, T.; Axelsson, A.-K. Pyrochlore Range from Bi2O3–Fe2O3–TeO3 System for LTCC and Photocatalysis and the Crystal Structure of New $Bi_3(Fe_{0.56}Te_{0.44})_3O_{11}$. *J. Am. Ceram. Soc.* **2012**, *95*, 644–650. [CrossRef]

16. Valant, M.; Suvorov, D. The Bi2O3-Nb2O5-NiO Phase Diagram. *J. Am. Ceram. Soc.* **2005**, *88*, 2540–2543. [CrossRef]

17. Khaw, C.C.; Tan, K.B.; Lee, C.K.; West, A.R. Phase equilibria and electrical properties of pyrochlore and zirconolite phases in the Bi_2O_3–ZnO–Ta_2O_5 system. *J. Eur. Ceram. Soc.* **2012**, *32*, 671–680. [CrossRef]

18. Chon, M.P.; Tan, K.B.; Khaw, C.C.; Zainal, Z.; Taufiq-Yap, Y.H.; Chen, S.K.; Tan, P.Y. Subsolidus phase equilibria and electrical properties of pyrochlores in the Bi_2O_3–CuO–Ta_2O_5 ternary system. *J. Alloys Compd.* **2016**, *675*, 116–127. [CrossRef]

19. Egorysheva, A.V.; Ellert, O.G.; Maksimov, Y.V.; Volodin, V.D.; Efimov, N.N.; Novotortsev, V.M. Subsolidus phase equilibria and magnetic characterization of the pyrochlore in the Bi_2O_3–Fe_2O_3–Sb_2O_x system. *J. Alloys Compd.* **2013**, *579*, 311–314. [CrossRef]

20. Lomakin, M.S.; Proskurina, O.V.; Sergeev, A.A.; Buryanenko, I.V.; Semenov, V.G.; Voznesenskiy, S.S.; Gusarov, V.V. Crystal structure and optical properties of the Bi–Fe–W–O pyrochlore phase synthesized via a hydrothermal method. *J. Alloys Compd.* **2021**, *889*, 161598. [CrossRef]

21. Lufaso, M.W.; Vanderah, T.A.; Pazos, I.M.; Levin, I.; Roth, R.S.; Nino, J.C.; Provenzano, V.; Schenck, P.K. Phase formation, crystal chemistry, and properties in the system Bi2O3–Fe2O3–Nb2O5. *J. Solid State Chem.* **2006**, *179*, 3900–3910. [CrossRef]

22. Ismunandar; Kamiyama, T.; Oikawa, K.; Hoshikawa, A.; Kennedy, B.J.; Kubota, Y.; Kato, K. Static bismuth disorder in $Bi_2−x(CrTa)O_7−y$. *Mater. Res. Bull.* **2004**, *39*, 553–560. [CrossRef]

23. Zhuk, N.A.; Krzhizhanovskaya, M.G.; Koroleva, A.V.; Nekipelov, S.V.; Kharton, V.V.; Sekushin, N.A. Thermal Expansion. XPS Spectra. and Structural and Electrical Properties of a New $Bi_2NiTa_2O_9$ Pyrochlore. *Inorg. Chem.* **2021**, *60*, 4924–4934. [CrossRef] [PubMed]

24. Zhuk, N.A.; Krzhizhanovskaya, M.G.; Koroleva, A.V.; Nekipelov, S.V.; Sivkov, D.V.; Sivkov, V.N.; Lebedev, A.M.; Chumakov, R.G.; Makeev, B.A.; Kharton, V.V.; et al. Spectroscopic characterization of cobalt doped bismuth tantalate pyrochlore. *Solid State Sci.* **2022**, *125*, 106820. [CrossRef]

25. Jusoh, F.A.; Tan, K.B.; Zainal, Z.; Chen, S.K.; Khaw, C.C.; Lee, O.J. Novel pyrochlores in the Bi_2O_3-Fe_2O_3-Ta_2O_5 (BFT) ternary system: Synthesis. structural and electrical properties. *J. Mater. Res. Technol.* **2020**, *9*, 11022–11034. [CrossRef]

26. Zhuk, N.A.; Sekushin, N.A.; Semenov, V.G.; Fedorova, A.V.; Selyutin, A.A.; Krzhizhanovskaya, M.G.; Lutoev, V.P.; Makeev, B.A.; Kharton, V.V.; Sivkov, D.N.; et al. Dielectric properties, Mössbauer study, ESR spectra of $Bi_2FeTa_2O_{9.5}$ with pyrochlore structure. *J. Alloys Compd.* **2022**, *903*, 163928. [CrossRef]

27. Matsuda, C.K.; Barco, R.; Sharma, P.; Biondo, V.; Paesano, A.; da Cunha, J.B.M.; Hallouche, B. Iron-containing pyrochlores: Structural and magnetic characterization. *Hyperfine Interact.* **2007**, *175*, 55–61. [CrossRef]

28. Filoti, G.; Rosenberg, M.; Kuncser, V.; Seling, B.; Fries, T.; Spies, A.; Kemmler-Sack, S. Magnetic properties and cation distribution in iron containing pyrochlores. *J. Alloys Compd.* **1998**, *268*, 16–21. [CrossRef]

29. Whitaker, M.J.; Marco, J.F.; Berry, F.J.; Raith, C.; Blackburn, E.; Greaves, C. Structural and magnetic characterisation of the pyrochlores $Bi_{2−x}Fe_x(FeSb)O_7$, (x=0.1, 0.2, 0.3), $Nd_{1.8}Fe_{0.2}(FeSb)O_7$ and $Pr_2(FeSb)O_7$. *J. Solid State Chem.* **2013**, *198*, 316–322. [CrossRef]

30. Jusoh, F.A.; Tan, K.B.; Zainal, Z.; Chen, S.K.; Khaw, C.C.; Lee, O.J. Investigation of structural and dielectric properties of subsolidus bismuth iron niobate pyrochlores. *J. Asian Ceram. Soc.* **2020**, *8*, 957–969. [CrossRef]

31. Jusoh, F.A.; Tan, K.B.; Zainal, Z.; Chen, S.K.; Khaw, C.C.; Lee, O.J.; Balachandran, R.; Ananda Murthy, H.C. Novel pyrochlore-structured bismuth iron antimonates: Structural. impedance and electrochemical studies. *Results Phys.* **2021**, *27*, 104542. [CrossRef]

32. Zhuk, N.A.; Krzhizhanovskaya, M.G.; Koroleva, A.V.; Semenov, V.G.; Selyutin, A.A.; Lebedev, A.M.; Nekipelov, S.V.; Sivkov, D.V.; Kharton, V.V.; Lutoev, V.P.; et al. Fe, Mg-Codoped Bismuth Tantalate Pyrochlores: Crystal Structure, Thermal Stability, Optical and Electrical Properties, XPS, NEXAFS, ESR, and 57Fe Mössbauer Spectroscopy Study. *Inorganics* **2023**, *11*, 8. [CrossRef]

33. Lebedev, A.M.; Menshikov, K.A.; Nazin, V.G.; Stankevich, V.G.; Tsetlin, M.B.; Chumakov, R.G. NanoPES Photoelectron Beamline of the Kurchatov Synchrotron Radiation Source. *J. Surf. Investig. X-ray Synchrotron Neutron Technol.* **2021**, *15*, 1039–1044. [CrossRef]

34. Zhuk, N.A.; Krzhizhanovskaya, M.G.; Belyy, V.A.; Kharton, V.V.; Chichineva, A.I. Phase transformations and thermal expansion of α- and β-BiTaO4 and the high-temperature modification γ-BiTaO4. *Chem. Mater.* **2020**, *32*, 5493–5501. [CrossRef]

35. Shannon, R.D. Revised effective ionic radii and systematic studies of interatomic distances in halides and chalcogenides. *Acta Crystallogr. A* **1976**, *32*, 751–767. [CrossRef]

36. Zhuk, N.A.; Lutoev, V.P.; Lysyuk, A.Y.; Makeev, B.A.; Belyy, V.A.; Nekipelov, S.V.; Sivkov, V.N.; Koroleva, A.V.; Krzhizhanovskaya, M.G.; Beznosikov, D.S. Thermal behavior. magnetic properties. ESR. XPS. Mössbauer and NEXAFS study of Fe-doped $CaCu_3Ti_4O_{12}$ ceramics. *J. Alloys Compd.* **2021**, *855*, 157400. [CrossRef]

37. Zhuk, N.A.; Lutoev, V.P.; Belyy, V.A.; Makeev, B.A.; Beznosikov, D.S.; Nekipelov, S.V.; Yermolina, M.V. EPR and NEXAFS spectroscopy of $BiNb_{1-x}Fe_xO_{4-\delta}$ ceramics. *Phys. B Condens. Matter* **2019**, *552*, 142–146. [CrossRef]

38. Allred, A.L.; Rochow, E.G. A scale of electronegativity based on electrostatic force. *J. lnorg. Nucl. Chem.* **1958**, *5*, 264–268. [CrossRef]

39. Regan, T.J.; Ohldag, H.; Stamm, C.; Nolting, F.; Luning, J.; Stöhr, J.; White, R.L. Chemical effects at metal/oxide interfaces studied by X-ray-absorption spectroscopy. *Phys. Rev. B* **2001**, *64*, 214422. [CrossRef]

40. Schuhl, Y.; Baussart, H.; Delobel, R.; Le Bras, M.; Leroy, J.-M.; Gengembre, L.; Grimblot, J. Study of mixed-oxide catalysts containing bismuth. vanadium and antimony. Preparation. phase composition. spectroscopic characterization and catalytic oxidation of propene. *J. Chem. Soc. Faraday Trans. 1* **1983**, *79*, 2055–2069. [CrossRef]

41. Biesinger, M.C.; Lau, L.W.M.; Gerson, A.R.; Smart, R.S.C. Resolving surface chemical states in XPS analysis of first row transition metals. oxides and hydroxides: Sc. Ti. V. Cu and Zn. *Appl. Surf. Sci.* **2010**, *257*, 887–898. [CrossRef]

42. Sarma, D.D.; Rao, C.N.R. XPES studies of oxides of second- and third-row transition metals including rare earths. *J. Electron. Spectrosc. Relat. Phenom.* **1980**, *20*, 25–45. [CrossRef]

43. Kasatikov, S.; Filatova, E.; Sakhonenkov, S.; Konashuk, A.; Makarov, A. Relationship between Ta Oxidation state and Its Local Atomic Coordination Symmetry in a Wide Range of Oxygen Non-stoichiometry Extent of TaOx. *J. Phys. Chem. C.* **2019**, *123*, 6849–6860. [CrossRef]

44. Yamashita, T.; Hayes, P. Analysis of XPS spectra of Fe^{2+} and Fe^{3+} ions in oxide materials. *Appl. Surf. Sci.* **2008**, *254*, 2441–2449. [CrossRef]